



Immunomodulation and osseointegration activities of Na₂TiO₃ nanorods-arrayed coatings doped with different Sr content

Dongmei Yu^{a,1}, Shuo Guo^{b,c,1}, Meng Yu^{a,1}, Wenwen Liu^b, Xiaokang Li^b, Dafu Chen^d, Bo Li^{a,**}, Zheng Guo^{b,***}, Yong Han^{a,*}

^a State Key Laboratory for Mechanical Behavior of Materials, Xi'an Jiaotong University, Xi'an, 710049, Shaanxi, China

^b Department of Orthopaedics, Tangdu Hospital, Fourth Military Medical University, Xi'an, 710038, Shaanxi, China

^c Department of Biomedical Engineering, Fourth Military Medical University, Xi'an, 710032, Shaanxi, China

^d Laboratory of Bone Tissue Engineering, Beijing Research Institute of Traumatology and Orthopaedics, Beijing Jishuitan Hospital, Beijing, 100035, China

ARTICLE INFO

Keywords:

Nanorods-patterned array
Sr incorporation
Macrophage polarization
Osteogenetic function of osteoblast
Osseointegration

ABSTRACT

To endow Ti-based orthopedic implants immunomodulatory capability and thus enhanced osseointegration, different amounts of Sr are doped in Na₂TiO₃ nanorods in the arrays with identical nanotopographic parameters (rod diameter, length and inter-rod spacing) by substitution of Na⁺ using hydrothermal treatment. The obtained arrays are denoted as STSr2, STSr4, and STSr7, where the arabic numbers indicate the incorporating amounts of Sr in Na₂TiO₃. The modulation effects of the Sr-doped nanorods arrays on macrophage polarization and osteogenetic functions of osteoblasts are investigated, together with the array without Sr (ST). Moreover, osseointegration of these arrays are also assayed in rat femoral condyles. Sr-doped nanorods arrays accelerate M1 (pro-inflammatory phenotype)-to-M2 (anti-inflammatory phenotype) transformation of the adhered macrophages, enhancing secretion of pro-osteogenetic cytokines and growth factors (TGF-β1 and BMP2), moreover, the Sr doped arrays directly enhance osteogenetic functions of osteoblasts. The enhancement of paracrine of M2 macrophages and osteogenetic function of osteoblasts is promoted with the increase of Sr incorporating amounts. Consequently, Sr doped arrays show significantly enhanced osseointegration *in vivo* compared to ST, and STSr7 exhibits the best performance. Our work sheds a new light on the design of surface chemical components and structures for orthopedic implants to enhance their osseointegration.

1. Introduction

Ti-based orthopedic implants is required to achieve osseointegration within a short period in clinic [1,2]. During the physiological process of osseointegration, macrophage mediated immune response plays a key role [3–5]. It is because that macrophages reveal two kinds of phenotypes, M1 and M2 [6–8]. Pro-inflammatory M1 macrophages with typical surface marker CC-chemokine receptor-7 (CCR-7), secrete cytokines such as interleukin-1β (IL-1β), interferon-γ (IFN-γ) and inducible nitric oxide synthase (iNOS) to provoke inflammation, resulting in bone absorption and fibrous encapsulation [9–11]; anti-inflammatory M2 macrophages with typical surface marker cluster of differentiation 206

(CD206), produce cytokines including IL-4, IL-10 and arginase 1 (Arg-1) to resolve inflammation and enhance osteogenesis [9,11,12] and also secrete transforming growth factor-β1 (TGF-β1) and bone morphogenetic protein 2 (BMP2) to induce migration, recruitment and osteogenetic differentiation of mesenchymal stem cells (MSCs) [12–15]. Consequently, to realize high osseointegration efficacy of Ti-based implants, surface modification is required to endow the implants with the ability of accelerating macrophage phenotypic transition from M1 phenotype to M2 phenotype, i.e., osteoimmunomodulatory capability.

Emerging evidences have shown that surface nanotopographies on Ti-based implants is of importance in mediating macrophage phenotypes [9,16–19]. For instance, nanopatterned grooves drove macrophages

Peer review under responsibility of KeAi Communications Co., Ltd.

* Corresponding author.

** Corresponding author.

*** Corresponding author.

E-mail addresses: libo1137@xjtu.edu.cn (B. Li), guozheng@fmmu.edu.cn (Z. Guo), yonghan@mail.xjtu.edu.cn (Y. Han).

¹ Co-first authors: These authors contributed equally to this work.

<https://doi.org/10.1016/j.bioactmat.2021.08.033>

Received 3 August 2021; Received in revised form 30 August 2021; Accepted 30 August 2021

Available online 2 September 2021

2452-199X/© 2021 The Authors. Publishing services by Elsevier B.V. on behalf of KeAi Communications Co. Ltd. This is an open access article under the CC

BY-NC-ND license (<http://creativecommons.org/licenses/by-nc-nd/4.0/>).

polarizing towards anti-inflammatory M2 phenotype [20]; 2-dimensional (2D) honeycomb-like TiO₂ micro-pores with nanosized pore-diameter (~90 nm) were more favored in mediating macrophages towards M2 phenotype compared to those with sub-micrometer sized pores [19]; 3-dimensional (3D) nanorods-patterned arrays accelerated macrophage phenotypic transformation towards M2 more efficiently compared to 2D microporous coating [21] and flat Ti [9]; more crucially, our previous work revealed that nanorods-patterned array with inter-rod spacing value of 75 nm showed significantly enhanced role in M1-to-M2 transformation of macrophage relative to the arrays with identical rod diameters and lengths but sub-micron inter-rod spacing values [10,18]. These aforementioned results provide the concept of constructing nanorods-patterned array with appropriate geometric parameters to accelerate phenotypic transition of macrophages from M1 to M2.

Besides nanotopographical cue, studies have also highlighted the significance of inorganic ions (such as Sr²⁺ [22,23], Mg²⁺ [24,25] and Zn²⁺ [26]) in controlling polarization behavior of macrophages. Among these ions, Sr²⁺ exhibits great potential in accelerating phenotypic transition of macrophages towards M2 compared to other inorganic ions [27]. For instance, Sr contained silica-based bioactive materials facilitated phenotypic transformation of macrophages towards M2 by the released Sr²⁺ to secrete abundant platelet-derived growth factor-BB (PDGF-BB), enhancing angiogenesis and thus osseointegration [28,29]. Owing to the Sr²⁺ and Zn²⁺ release, Sr–Zn–P coating on Ti preferentially polarized macrophages towards M2 phenotype by activating HIF-1 signaling pathway, leading to the enhanced osseointegration of Ti-based implant in rat femur [30]. Moreover, Sr²⁺ exhibits modulatory effects not only on polarization behavior of macrophages but also on osteogenic function of osteogenesis-related cells. For instance, Sr²⁺ upregulated adhesion, proliferation and osteogenic differentiation of MSCs [27,31,32] through activating extracellular regulated protein kinases (ERK)/mitogen-activated protein kinase (MAPK) and/or Wnt signaling pathway [33,34]. However, our previous work showed that the enhanced role in osteogenesis of Sr-doped hydroxyapatite coating on Ti was dependent on the doped amounts of Sr²⁺, revealing higher amount of doped Sr²⁺ inducing more significant osteogenesis [35]. Although recent work has shown that different amounts of Sr²⁺ contained in culture medium could induce different polarization behaviors of macrophages [29,36,37], the immunomodulation and subsequent osseointegration of nanorods-patterned coatings doped with different Sr content have not been illustrated yet.

In the present study, sodium titanate (ST) nanorods arrays with identical rod diameter, length and inter-rod spacing value but doped with different Sr content were constructed on Ti. The regulatory effects of these arrays on macrophage polarization and osteogenic functions of osteoblasts were assayed respectively using separate culture and co-culture systems, moreover, osseointegration of these arrays were also examined in rats femoral condyles.

2. Experimental methods

2.1. Fabrication of strontium-incorporated sodium titanate coatings

ø14 × 2 mm sized pure Ti discs and M1.7 × 4 mm sized pure Ti screws were machined and cleaned. To construct Na₂TiO₃ nanorods arrays, each disc or screw was soaked in 10 mL NaOH solution (1 M) contained in a Teflon-lined autoclave to undergo hydrothermal treatment (HT) for 1.5 h at 100 °C. Subsequently, the hydrothermal treated sample was immersed in NaOH solution (0.5 M) to undergo another HT at 220 °C for 4 h, and the resultant coating is termed as ST.

For Sr-doped ST with different Sr content, ST coated Ti were received ion exchange at 100 °C for 24 h in 10 mL Sr(CH₃COO)₂ aqueous solution with different concentrations of 0.1, 10 and 1000 mM, and these resultant Sr-doped coatings were respectively termed as STSr2, STSr4 and STSr7. All the samples for biological experiments were sterilized with cobalt 60 irradiation for 48 h.

2.2. Characterization of coating structure

The morphologies and chemical components of formed nanorods arrays were observed under a scanning electron microscope (SEM; SU6600, Japan) affiliated with energy dispersive X-ray spectrometer (EDX). The geomorphological parameters of the nanorods, including inter-rod spacing, rod diameter and length, were examined with Image J (Pawak Incorporation, Germany) from surface and cross-sectional SEM images. Four random areas were measured to get the average values. Phase compositions was identified by an X-ray diffractometer in thin film model (XRD; XRD- 7000, Japan) over a 2θ angle of 20–80°. An individual nanorod scratched from each kind of nanorods arrays was characterized by a transmission electron microscope (TEM; G2F30, USA) equipped with EDX in STEM model. The element composition and chemical bonds of the arrays were identified using an X-ray photoelectron spectroscopy (XPS; Thermo Electron Corporation, USA), with Al Kα radiation and photoelectron take-off angle of 45°. C1s peak with 284.6 eV binding energy was used to calibrate peak positions.

2.3. Ion release

The nanorods-arrayed coatings were respectively soaked in 50 mL physiological saline (PS, 0.9 wt% NaCl) at 37 °C for 1, 3, 7, 14, 30, and 60 d. Sr concentrations of sample-immersed solutions were detected using an inductively coupled plasma-mass spectrometry (ICP-MS; Agilent 7700, U.S.A.). The release profiles were acquired from five replicates for each kind of the sample-immersed solutions at each immersion time.

2.4. Cell culture

RAW 264.7 macrophage and mouse pre-osteoblast cell, MC3T3, purchased from Chinese Academy of Sciences were employed in subsequent *in vitro* biological tests. Macrophages were incubated in 10% fetal bovine serum (FBS; Gibco, USA) and 1% penicillin/streptomycin (Gibco, U.S.A.) contained Dulbecco's modified Eagle's medium (DMEM; Gibco, U.S.A.). MC3T3 were incubated in Minimum Essential Medium α (α-MEM; Gibco, U.S.A.) with 10% FBS (Gibco, U.S.A) and 1% antibiotics (Gibco, USA). Both cells were cultured at 37 °C in a humidified incubator filled with 5% CO₂ with refreshing the culture media of the cells every other day.

2.5. Behavior of macrophages or MC3T3 seeded on bare and nanorods-arrayed Ti

Macrophages or MC3T3 were respectively seeded on the bare and nanorods-arrayed Ti discs centrally put into tissue culture plates (TCP) with 24 wells with a density of 2 × 10⁴ cells/well and incubated for different time. After one day of incubation, the cells adhered on the samples were fixed with 4% paraformaldehyde, dehydrated with gradient ethanol and spraying gold, and then the adhered cell morphologies were observed using SEM (SU6600, Japan). Cytoskeleton, vinculin and nuclei of cells cultured on the samples were stained using FAK100 kit (Abcam, U.S.A.). Briefly, the cells adhered on the samples were rinsed with PBS, followed by fixing with 4% paraformaldehyde and staining with the kits. The fluorescence-stained samples were observed with a laser scanning confocal microscope (LSCM; FV1200, Olympus, Japan).

To examine modulation effects of the samples on macrophage polarization, mRNA expressions of CCR-7 and CD206 in macrophages incubated on samples for 1, 3, 7 days were detected with real-time quantitative polymerase chain reaction (RT-qPCR; LightCycler@96, Roche, Switzerland). Typically, total cellular RNA was isolated with TRIZOL reagent (Invitrogen, U.S.A.) and converted into cDNA with the Reverse Transcription Reagents Kit (Takara, Japan) following the instruction of manufacturer. Glyceraldehyde-3-phosphate dehydrogenase (GAPDH) was used as an endogenous reference gene. The primer sequences of the tested genes in this work were displayed in Table 1.

Furthermore, fluorescence staining assays of proteins, iNOS and Arg-1, were carried out to visualize polarized macrophages. The macrophages seeded on the discs for 3 days were fixed using 4% paraformaldehyde at 4 °C for 30 min. After fixation, the cells were permeated with 0.1% Triton X-100 for 10 min followed by blocking with 5% bovine serum albumin for 1 h. Rabbit anti-mouse primary antibody of iNOS with dilution ratio of 100 (Abcam, U.S.A) and goat anti-mouse primary antibody of Arg-1 with dilution ratio of 100 (Abcam, U.S.A) were applied to incubate cells adhered on the samples at 4 °C overnight. After that, respective fluorescence labelled secondary antibodies, donkey anti-rabbit IgG antibody (Bioss, China) with dilution ratio of 200 and donkey anti-goat IgG antibody (Bioss, China) with dilution ratio of 200, were applied to label the markers, and iNOS was marked in green, Arg-1 was marked in red. Nuclei were marked in blue color using 4, 6-diamidino-2-phenylindole (DAPI; Servicebio, China). The fluorescence-labelled cells were observed using LSCM (FV1200, Olympus, Japan).

IL-1 β and IFN- γ , IL-4 and IL-10 as well as TGF- β 1 and BMP2 in the supernatant of culture media secreted by macrophages at 1, 3 and 7 d of incubation were detected with corresponding Enzyme-linked immunosorbent assay kits (ELISA; Thermo Fisher Scientific, U.S.A.).

The osteogenic mRNA expressions in MC3T3 cultured on discs for 3, 7 and 14 d, such as runt-related transcription factor 2 (Runx2), osteopontin (OPN) and osteocalcin (OCN), were detected with RT-qPCR. Corresponding genes expressions were normalized to GAPDH and the primer sequences of the tested genes were exhibited in Table 1.

2.6. MC3T3 co-cultured with macrophages adhered on the samples

A transwell chamber system was applied to evaluate osteogenic behavior of MC3T3 co-cultured with macrophages seeded on the discs. Macrophages were inoculated on the samples with a density of 2×10^4 cells/well in TCP with 24 wells. 8 μ m pore sized membrane filters were gently mounted above 24-well TCP and MC3T3 (2×10^4 cells/well) were seeded in the upper chamber. After co-culturing for predetermined time, the MC3T3 on top side of permeable membrane were carefully removed using cotton swabs, while the cells adhered on the bottom surface of permeable membrane were tested in following experiments. The gene expressions of Runx2, OPN and OCN in MC3T3 co-cultured with macrophages seeded on bare and nanorods-arrayed Ti discs for 3, 7 and 14 d were assayed with RT-qPCR. Alkaline phosphatase (ALP) and Alizarin Red staining of MC3T3 migrated to the bottom surface of permeable membrane was respectively performed at days 3 and 14 after co-culturing with macrophage on the samples. Briefly, the cells were fixed with 4% paraformaldehyde and stained with ALP and Alizarin Red staining kits (Servicebio, China) followed by observing with a microscope (Olympus IX 73, Japan). 5 images were captured from randomly selected areas on the permeable membrane.

2.7. Animals and in vivo implantation

Surgical operations on experimental animals were identified by Institutional Lab Animal Centre and Ethics committee of Fourth Military Medical University and conducted according to animal welfare requirements. After clinical check, forty-five eight-week-old SD rats (male, ~200 g/rat) were allocated into five groups (nine per group) randomly

Table 1
Sequences of genes primers.

Gene	Forward primer sequence (5'-3')	Reverse primer sequence (5'-3')
CCR7	TGAGGTCACGGACGATTACAT	GTAGGCCACGAAACAATGAT
CD206	CTCTGTTTCAGCTATTGGACGC	CGGAATTCTGGGATTCAGCTTC
Runx2	GAACCAAGAAGGCACAGACAGA	GGCGGGACACCTACTCTCATAC
OPN	TACGACCATGAGATTGGCAGTGA	TATAGGATCTGGGTCAGGCTGTA
OCN	ACCATCTTCTGCTCACTCTGCT	CCTTATTGCCCTCCTGCTTG
GAPDH	AGTTCGGTGTGAACGGATTTC	TGTAGACCATGTAGTTGAGGTCA

for implantation. The rats were intraperitoneally injected 20 mg pentobarbital sodium solution for anesthesia. For each rat, two $\phi 1.5 \times 4$ mm sized holes were drilled on both sides of femoral condyles for screw implantation (one implant per femoral condyle), followed by skin suture. All the post-implantation rats were intramuscularly injected penicillin for 3 days to prevent infection.

An overdose of anesthesia was used to sacrifice the rats respectively at 2, 4, and 6 w of post-surgery. Sixty femoral condyles containing screws (twelve per group) were harvested and subsequently examined with micro-computed tomography (Micro-CT; Y.CHEETAH, Germany) under the parameters of 90 kV, 50 μ A and scanning resolution of 7 μ m to evaluate peri-implant new bone. The obtained data were analyzed using micro-CT machine equipped VG Studio MAX software. For histological examination, each of the femoral condyles containing screws was fixed and dehydrated, followed by embedding in polymethyl methacrylate (PMMA) for cutting into 150 μ m thick sections (Leitz 1600, Germany). The obtained sections were thinned into 20 μ m thick foils and polished for Van Gieson's picric-fuchsin (VG) staining. These stained sections were observed using a microscope (Olympus IX 73, Japan) followed by analyzing with Image Pro Plus software (IPP).

In addition, screws contained in other thirty femoral condyles (six per group) were removed. Subsequently, the left femoral condyles were fixed (4% paraformaldehyde), decalcified (10% EDTA solution) and dehydrated (gradient ethanol) followed by embedding in paraffin. 5 μ m thick sections were cut (Leica, Germany), followed by staining with Hematoxylin and eosin (HE) dye solution set and Masson dye solution set (Servicebio, China). HE and Masson staining images were captured using a Panoramic scanner (250/MIDI, Hungary) and the acquired images were quantitatively evaluated using IPP.

2.8. Statistical analysis

Experimental data collected was quantitatively evaluated with SPSS 19.0 software and presented in the form of means \pm standard deviation. The determination of significance was carried out using one-way ANOVA and Student-Newman-Keuls post hoc tests, and p value < 0.05 was considered significant and p value < 0.01 was considered to be highly significant.

3. Results and discussion

3.1. Structural characterization of Sr-doped nanorods arrays

Fig. 1a exhibits the surface morphologies of these HT derived nanorods-patterned arrays, which exhibit similar geometric parameters with rod diameter of 65.10 ± 4.53 nm and inter-rod spacing of 75.20 ± 4.64 nm. Based on the EDX spectrum of Ti, O and Na detected on the cross-sectional views of these arrays, it is revealed that these nanorods in arrays are quasi-upright aligned on Ti substrates with similar length of 2.00 ± 0.15 μ m. As confirmed by XRD (Fig. 1b), the four kinds of nanorods-patterned arrays compose of sodium titanate (Na_2TiO_3 , shortened as ST), while (1 1 2), (2 1 1) and (2 0 0) diffraction peaks detected on the nanorods-patterned arrays underwent ion exchange in Sr-contained solution shift to a lower angle compared to the array formed without ion exchange. Moreover, the shift to lower angle tends to be more obvious with the increase in Sr^{2+} concentration in the solutions used for ion exchange. The results indicate the successful incorporation of Sr in these nanorods, which are further confirmed by TEM. Fig. 1c show the TEM images of an individual nanorod obtained from the array underwent ion exchange in 10 mM strontium acetate contained solution as a representative. The selected area electron diffraction (SAED), high-resolution TEM (HRTEM) image and EDX spectrum confirm that nanorod consists of Sr doped Na_2TiO_3 , and the doped Sr leads to the increase in interplanar spacing of Na_2TiO_3 [38]. Based on the atomic contents of the doped Sr in these nanorods detected by TEM (Table 2), the Sr-doped nanorods arrays are termed as STSr₂,

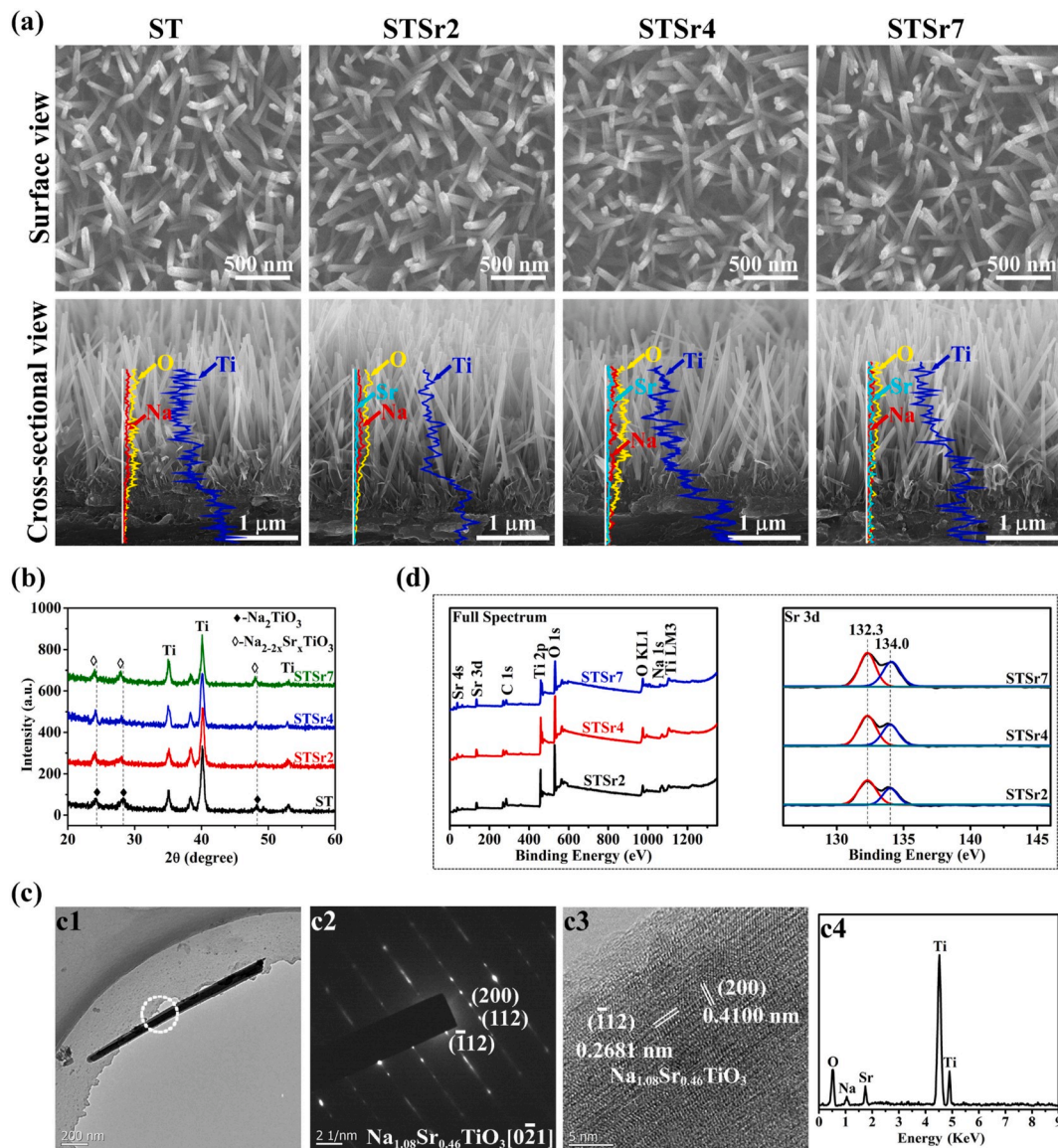


Fig. 1. (a) The morphologies of surfaces and cross-sections, EDX spectrum together with (b) XRD patterns of the HT derived arrays; (c) TEM images of an individual nanorod obtained from STSr4: (c1) panoramic bright-field image and (c2) SAED pattern, (c3) HRTEM image and (c4) EDX spectrum detected on the circle-dotted micro-region in (c1); (d) XPS full spectrum and high-resolution spectrum of Sr 3d detected on STSr2, STSr4 and STSr7.

STSr4 and STSr7, respectively, and the nanorods-patterned array with out Sr incorporation is named as ST. The successful incorporation of Sr in the nanorods-patterned arrays is also identified by XPS full spectrum together with high-resolution spectrum of Sr 3d as shown in Fig. 1d,

Table 2

Chemical compositions of individual nanorods obtained from the nanorods arrays examined using EDX equipped TEM.

Nanorod	Elemental composition (At.%)				Stoichiometric formula
	Ti	O	Na	Sr	
ST	17.0 ± 0.7	50.0 ± 0.7	33.0 ± 0.5	–	Na ₂ TiO ₃
STSr2	17.0 ± 0.8	50.0 ± 0.8	25.4 ± 0.4	7.6 ± 0.2	Na _{1.54} Sr _{0.23} TiO ₃
STSr4	16.9 ± 0.8	50.1 ± 0.9	17.8 ± 0.3	15.2 ± 0.3	Na _{1.08} Sr _{0.46} TiO ₃
STSr7	16.8 ± 0.9	50.1 ± 1.0	8.4 ± 0.2	24.7 ± 0.4	Na _{0.50} Sr _{0.75} TiO ₃

which depict increased intensities of Sr peaks in STSr2, STSr4 and STSr7, suggesting the tendency of gradually increased amounts of incorporated Sr in these coatings. Moreover, two peaks of Sr 3d respectively locate at 132.7 eV (3d_{5/2}) and 134.5 eV (3d_{3/2}), in agreement with SrTiO₃ in previous report [31], which is confirmed that Sr in the form of Sr²⁺ is incorporated into Na₂TiO₃ nanorods by the partial substitution of Na⁺ [39,40].

3.2. Sr²⁺ release from the Sr-doped nanorods arrays

Fig. 2 shows the Sr²⁺ release from the nanorods arrays incorporated with Sr during immersion. Obviously, Sr concentrations of the coatings immersed physiological solutions (PS, i.e., 0.9% NaCl) tend to significantly increase in the first 10 days and gradually reach stability, suggesting that Sr incorporated into these nanorods can be long-termly released into the PS solutions. Due to the different Sr incorporating amounts, the released amounts of Sr from these arrays follow the order of STSr7 > STSr4 > STSr2 at each immersion time point.

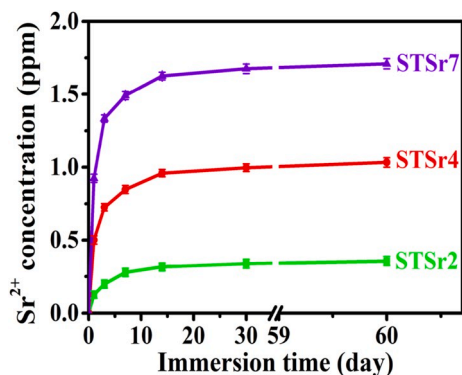


Fig. 2. Sr²⁺ concentrations of the PS solutions immersing STSr2, STSr4 and STSr7 with prolonging immersion time.

3.3. Phenotypic transition of macrophages on the nanorods arrays and bare Ti

Fig. 3a exhibits the morphologies of macrophages adhered on the nanorods arrays and bare Ti for 1 d. The macrophage adhered on Ti exhibits spherical morphology without pseudopod extension, while the macrophages adhered on the nanorods-patterned arrays are elongated with obvious filopodia compared to that on Ti, moreover, the cells on the Sr-doped nanorods arrays exhibit more pronounced elongation and more amounts of filopodia with the tendency of STSr7, STSr4 and STSr2. As known, cell adhesion and the assembly of filopodia and lamellipodia are mediated by the vinculin-associated formation of focal adhesion (FA) that functions as an adaptor protein of F-actin [41]. Thus, vinculin, F-actin and nuclei of macrophages adhered on these nanorods arrays and bare Ti for 1 d were visualized using fluorescent staining (Fig. 3b). Compared to Ti, nanorods-patterned arrays stimulate macrophages to secrete more vinculin (red color labelled) and F-actin (green color

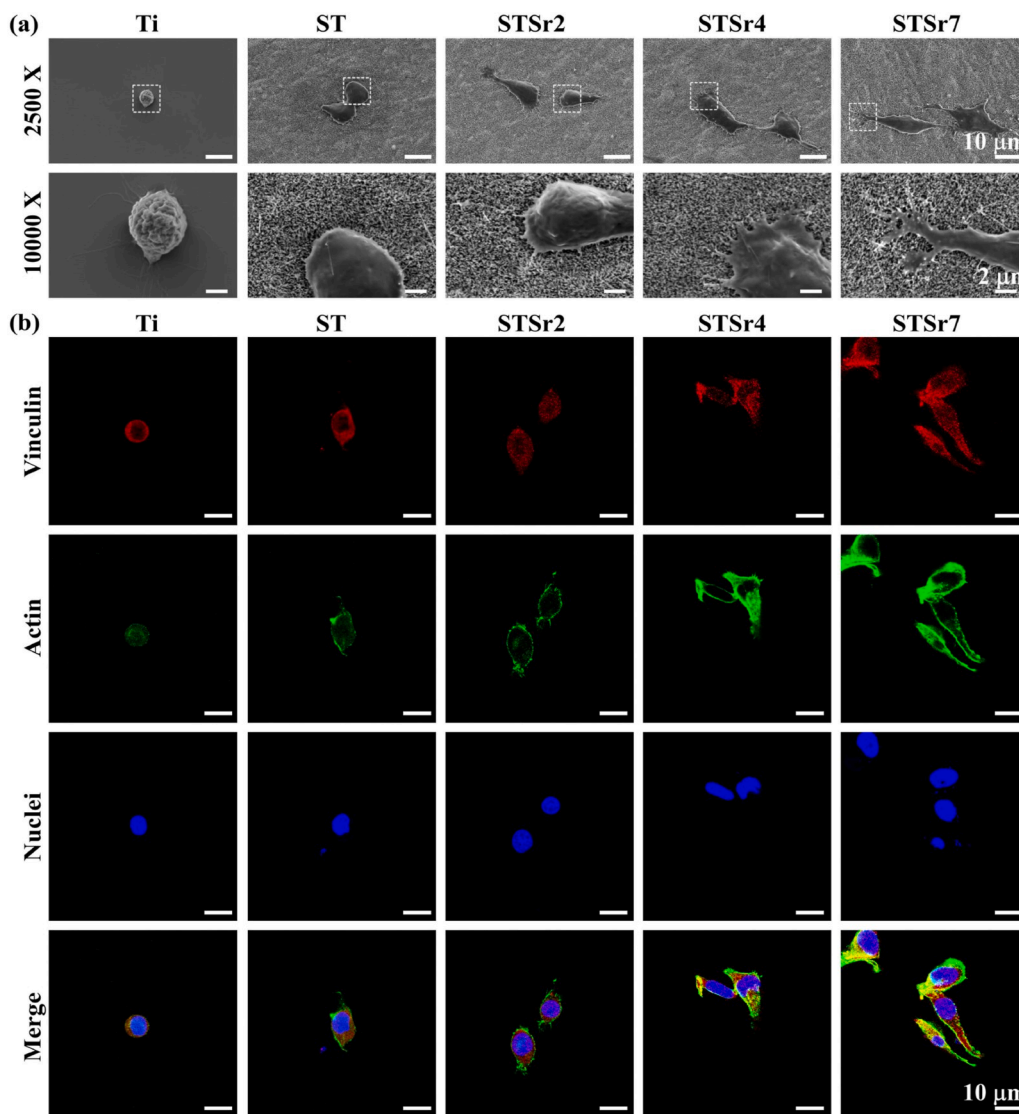


Fig. 3. (a) SEM morphology, (b) vinculin (marked in red), actin (marked in green) and nuclei (marked in blue) fluorescence-stained images of macrophages adhered on the nanorods arrays and bare Ti after 1 d of incubation.

labelled), and the enhancement is more significant for the cells on the Sr-doped arrays following the trend of STSr7, STSr4 and STSr2. Collectively, Sr-doped nanorods arrays significantly enhance macrophage adhesion and rapidly stimulate cell elongation compared to the array without Sr, which become more pronounced with increasing the amounts of incorporated Sr. This is attributed to that more amount of released Sr^{2+} from the array doped with higher content of Sr can enhance cellular integrins expression and subsequent FA formation to promote cell adhesion and pseudopod formation [42,43].

Our previous work revealed that macrophage morphology is associated with their polarization phenotypes. It is suggested that macrophages with M1 phenotype usually display round-like morphology, while macrophages with M2 phenotype exhibit spindle-like morphology with extended lamellipodia [9,18]. To determine the macrophage

phenotype, the gene expressions of CCR-7 and CD206 in macrophages adhered on the samples were detected and shown in Fig. 4a. The results reveal that the nanorods-patterned arrays are beneficial in polarizing macrophages towards M2 phenotype compared to Ti, as confirmed by the downregulated CCR-7 and upregulated CD206 in the cells at each time point. It is because of the enhanced cell adhesion and pseudopod formation by nanorods-patterned arrays significantly activates actin stress fibers (RhoA)/Rho-associated protein kinase (ROCK) signaling pathway to polarize macrophages towards M2 phenotype [18,19]. Moreover, the trend of the adhered macrophages polarizing towards M2 phenotype becomes more pronounced with the increased amounts of doped Sr in the nanorods. Fluorescence images of M1-featured cytokine, iNOS, and M2-featured cytokine, Arg-1, in the macrophages adhered on the nanorods and bare Ti for 3 days are photographically and statistically

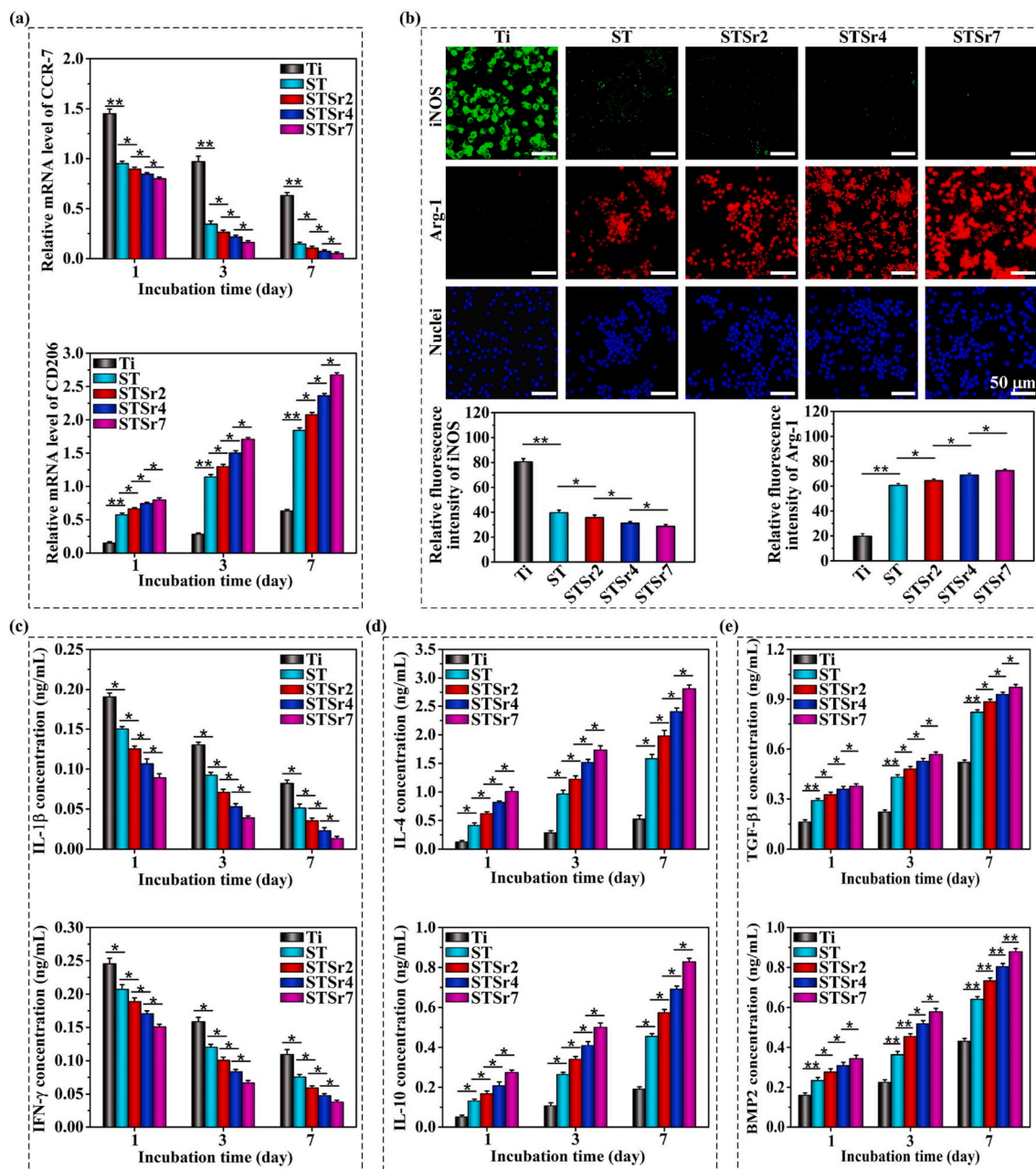


Fig. 4. Phenotype polarization of macrophages seeded on ST, STSr2, STSr4 and STSr7 and bare Ti: (a) inflammation-related gene expressions of CCR-7 and CD206 at 1, 3 and 7 days of incubation; (b) fluorescence images of iNOS (marked in green), Arg-1 (marked in red) and nuclei (marked in blue) together with the statistical fluorescent intensities of CCR-7 and Arg-1 to characterize their expressions at day 3 of incubation; secretion of (c) IL-1 β and IFN- γ , (d) IL-4 and IL-10 and (e) TGF- β 1 and BMP2 by macrophages incubated on the nanorods arrays and bare Ti for 1, 3 and 7 days. *p < 0.05, **p < 0.01.

shown in Fig. 4b. Ti induces macrophages to secrete much more amount of iNOS compared to the nanorods-patterned arrays, while the arrays provoke more secretion of Arg-1 by the macrophages following the trend of STSr7, STSr4, STSr2 and ST. The fluorescence staining results further confirmed the enhanced role of Sr-doped nanorods arrays in polarizing macrophages towards M2. Consequently, Sr doped arrays downregulate M1 macrophage secreted pro-inflammatory factors of IL-1 β and IFN- γ , as well as upregulate M2 macrophage secreted anti-inflammatory cytokines of IL-4 and IL-10 compared to ST and Ti at each incubation time point. Simultaneously, M2 macrophage secreted TGF- β 1 and BMP2 are highly expressed in the protein levels for Sr-doped nanorods arrays compared to ST and Ti, especially the arrays doped with higher Sr

amounts. Taken together, Sr doped arrays accelerate phenotypic transformation of the adhered macrophages towards M2 phenotype compared to the array without Sr and bare Ti, leading to the upregulation of M2 macrophage secreted anti-inflammatory cytokines and growth factors, and the acceleration tends to be more pronounced with the increase of Sr incorporating amounts.

3.4. Osteogenic behaviors of MC3T3 on bare and nanorods-patterned Ti

Adhesion behavior of osteoblasts, MC3T3 cultured on bare and nanorods-patterned Ti for 1 day was examined and shown in Fig. 5a. All the cells adhered on bare and nanorods-patterned Ti exhibit polygonal-

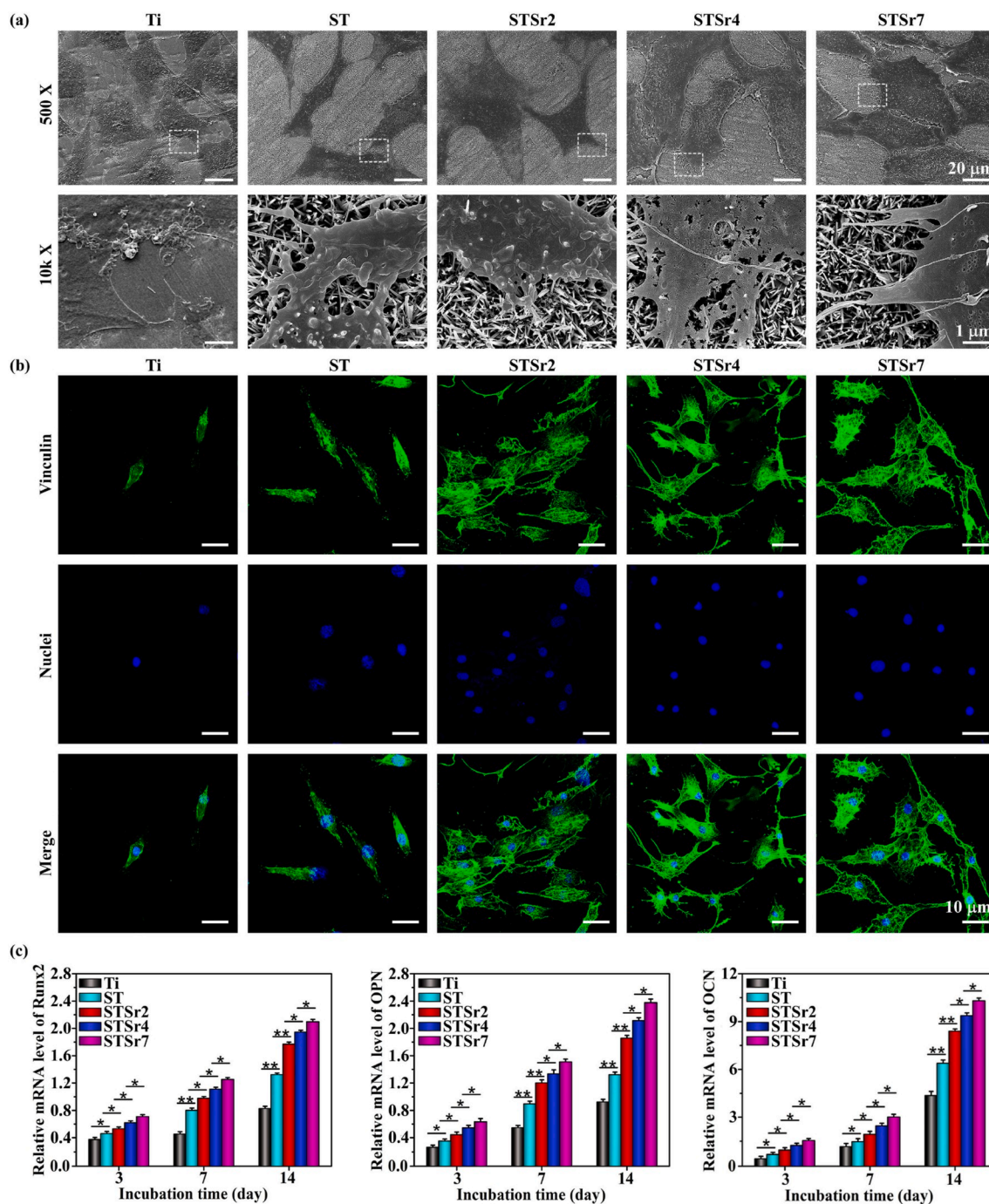


Fig. 5. Adhesion and osteogenic differentiation of MC3T3 incubated on ST, STSr2, STSr4 and STSr7 and bare Ti: (a) morphologies, and (b) fluorescence-stained vinculin (marked in green) and nuclei (marked in blue) of MC3T3 after culturing on the samples for 1 d; (c) expressions of osteogenesis-related genes (Runx2, OPN and OCN) in MC3T3 after culturing on the samples for 3, 7 and 14 d. * $p < 0.05$, ** $p < 0.01$.

like morphology but different in spread sizes and amounts of filopodia. Larger sized osteoblasts appear on nanorods-patterned Ti compared to Ti and the spreading size of cells increases with Sr incorporating amounts. Moreover, amplified images exhibit that more amounts of filopodia form at the borders of cells on the Sr doped arrays (especially on the array doped with higher amount of Sr) compared to ST and Ti. To further examine cell adhesion on the arrays, the vinculin and nuclei of MC3T3 adhered on the arrays and bare Ti for 1 day are stained and shown in Fig. 5b. The fluorescence images show that a few vinculin-denoted focal adhesion contacts appear in MC3T3 on Ti, however, many focal

adhesions formed in the cells on ST, while they are less than those on Sr doped arrays, which increase with Sr incorporating amounts in the nanorods. It is revealed that higher amount of released Sr upregulates the gene expressions of integrins subunits, such as $\alpha 2$, $\alpha 5$, and $\beta 1$ [44], which engage the cells and active focal adhesion kinase through binding to fibronectin to facilitate cell adhesion and filopodia formation [42,45]. It has been shown that the enhanced cell adhesion and filopodia formation plays a positive role in osteogenic differentiation of osteoblasts [46]. To identify the modulation effects of the arrays doped with different Sr amounts on osteoblastic differentiation, osteogenesis-related genes

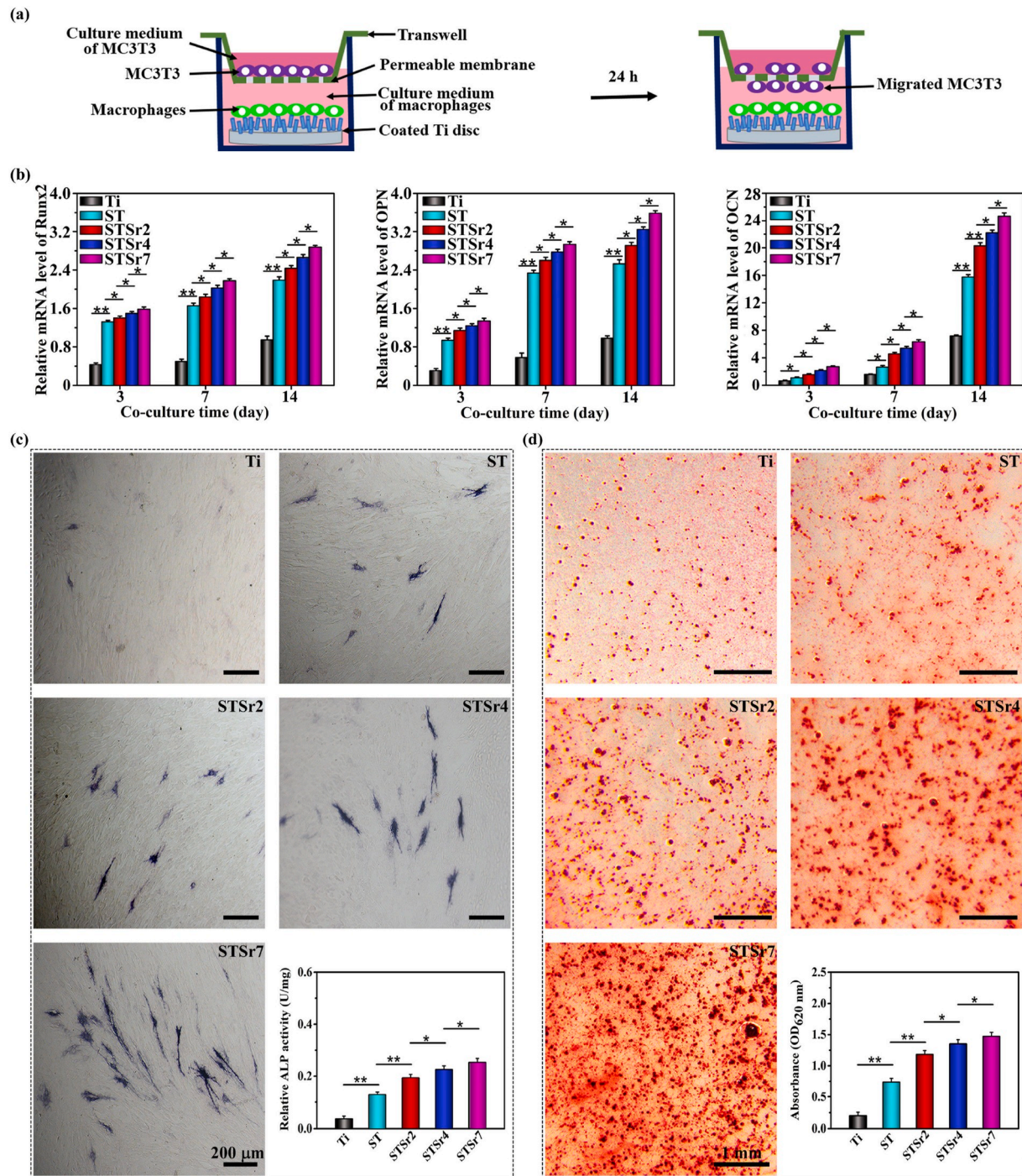


Fig. 6. Osteogenic differentiation and ECM mineralization of MC3T3 co-cultured with macrophages seeded on ST, STSr2, STSr4 and STSr7 and bare Ti: (a) schematic illustration showing the co-culture system; (b) expressions of osteogenic genes by MC3T3 co-cultured with macrophages adhered on the samples for 3, 7 and 14 days; (c) staining images and quantification of ALP activities of MC3T3 co-cultured with macrophages seeded on the samples for 3 days as well as (d) Alizarin Red staining images and quantification of mineralized nodules of MC3T3 co-cultured with macrophages seeded on the samples for 14 days. *p < 0.05, **p < 0.01.

expressions, including Runx2, OPN and OCN in MC3T3 incubated on the nanorods arrays and Ti for 3, 7 and 14 d were assayed (Fig. 5c). The gene expressions of Runx2, OPN and OCN in MC3T3 on the nanorods arrays and Ti are upregulated during the incubation period (3–14 days) but with

different magnitude. Their expressions in the cells on Sr doped arrays are significantly higher than those on ST and much higher than those on bare Ti at each incubation time point with the trend of STSr7, STSr4, STSr2, ST and Ti. Collectively, Sr incorporated into nanorods-patterned arrays

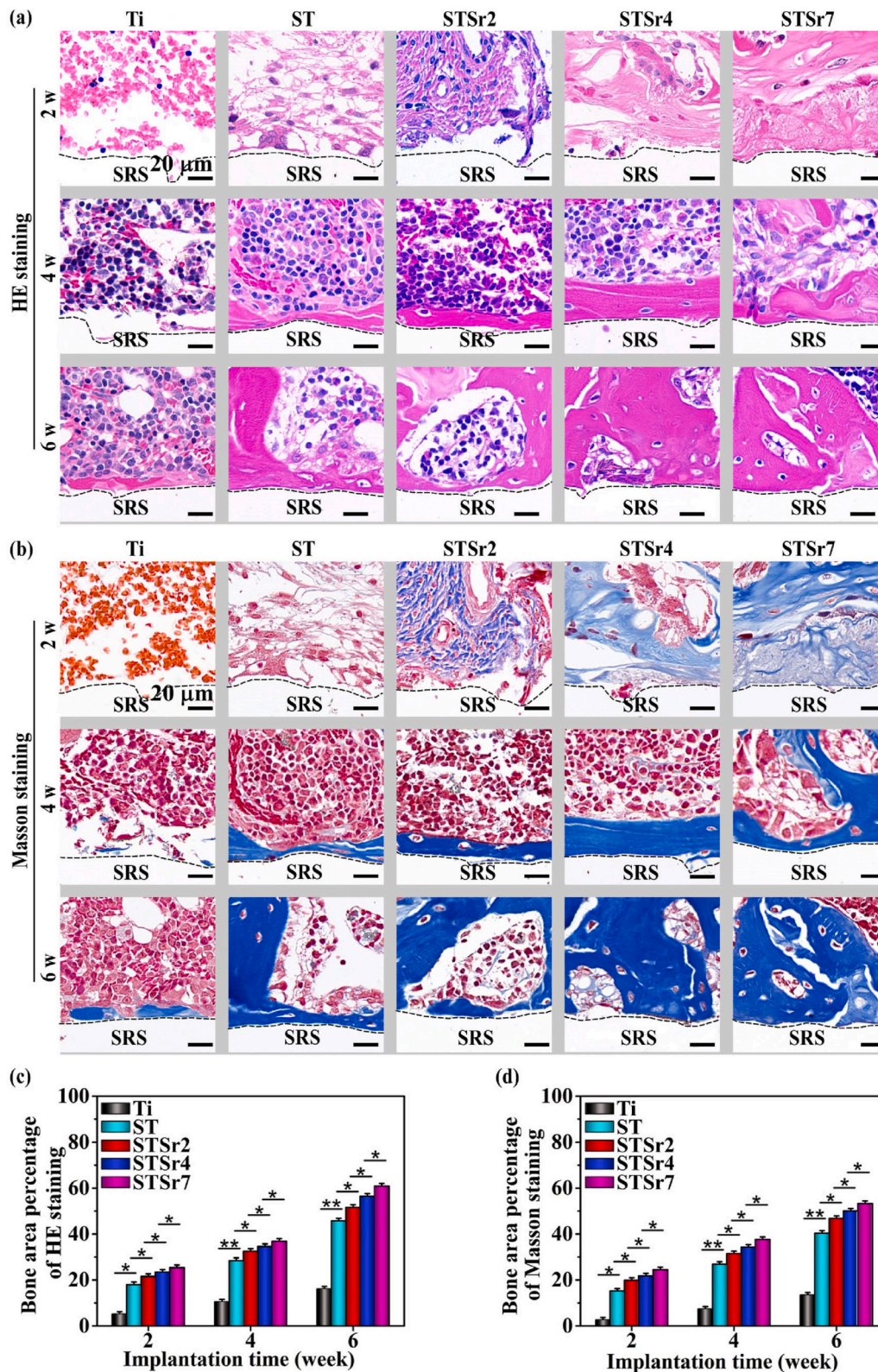


Fig. 7. HE and Masson staining analyses of the new bone surrounding the screws implanted in rat femoral condyles for 2, 4 and 6 weeks: (a) HE and (b) Masson staining images of new bone formed in the regions adjacent to the screws-removed spaces (SRS); (c) HE staining assayed and (d) Masson staining assayed qualification of new bone area to total area ratios. The black-dotted lines represent the boundaries between SRS and tissue. * $p < 0.05$, ** $p < 0.01$.

further enhance adhesion and subsequent osteogenic differentiation of osteoblasts compared to the array without Sr, and the enhancement tends to be more obvious with the increase of Sr incorporating amounts.

3.5. Osteogenesis of MC3T3 co-cultured with macrophages on the nanorods arrays and bare Ti

Given that osseointegration originates from macrophages polarization that sequentially regulates osteogenic cell recruitment and differentiation for osteogenesis [47], the osteogenetic function of MC3T3 in response to the mediators produced by macrophages seeded on the bare Ti and nanorods arrays was assessed in a transwell model, schematically shown in Fig. 6a. The osteogenic gene expressions (Runx2, OPN and OCN) and ALP activities in MC3T3 co-cultured with the macrophages seeded on the samples for 3, 7 and 14 days were shown in Fig. 6b and c. Compared to MC3T3 co-cultured with macrophages on bare Ti, osteogenic differentiation of MC3T3 co-cultured with macrophages on the nanorods arrays is significantly enhanced at each time point. Moreover, the enhancement is far more pronounced in response to macrophages on the Sr doped arrays, following the order of STSr7, STSr4 and STSr2. The extracellular matrix (ECM) mineralization at day 14 of MC3T3 in response to macrophages on the samples reveals the similar results (Fig. 6d). As known, M2 macrophage secreted IL-4, TGF- β 1, and BMP2 function as chemotactic factors to recruit osteogenesis-related cells [13, 48,49], moreover, IL-10 activates p38/MAPK signaling pathway to promote osteogenic differentiation of osteogenesis-related cells [50], and TGF- β 1 and BMP2 (especially the latter) strongly induce osteoblastic

differentiation of osteoblasts [14,15]. Consequently, Sr doped arrays derived increase in secretion amounts of M2-featured IL-4, IL-10, TGF- β 1 and BMP2 by the adhered macrophages (Fig. 4b and e) enhances osteogenetic differentiation of MC3T3, and the enhancement is increased with Sr incorporating amounts in the nanorods.

Notably, as shown in Fig. 5c vs. 6b-d, there is no difference in osteogenetic functions of MC3T3 between direct culturing on Ti and co-culturing with macrophages on Ti at each incubation time point. Nevertheless, osteogenetic functions of the osteoblasts co-cultured with macrophages on the nanorods arrays, especially on the Sr doped arrays with higher content, are significantly promoted than those of MC3T3 directly culturing on the corresponding arrays. It is indicated that the paracrine of macrophages, such as anti-inflammatory cytokines and pro-osteogenic growth factors, plays a more crucial role than nanotopography and released Sr²⁺ in enhancing osteogenetic functions of MC3T3.

3.6. Osseointegration of the nanorodspatterned arrays

Osseointegration driven by nanorods arrays and bare Ti were examined in rat femoral condyles at the time points of 2, 4 and 6 weeks after implantation (Figs. 7 and 8). After 2 weeks of implantation, no mature bone surrounding the bare Ti and nanorods-patterned arrays are observed in H&E and Masson stained sections (Fig. 7a and b). However, more organized and compact collagen fibers form around nanorods-patterned arrays (especially STSr7) compared to those around ST, which subsequently induce more compact structure and

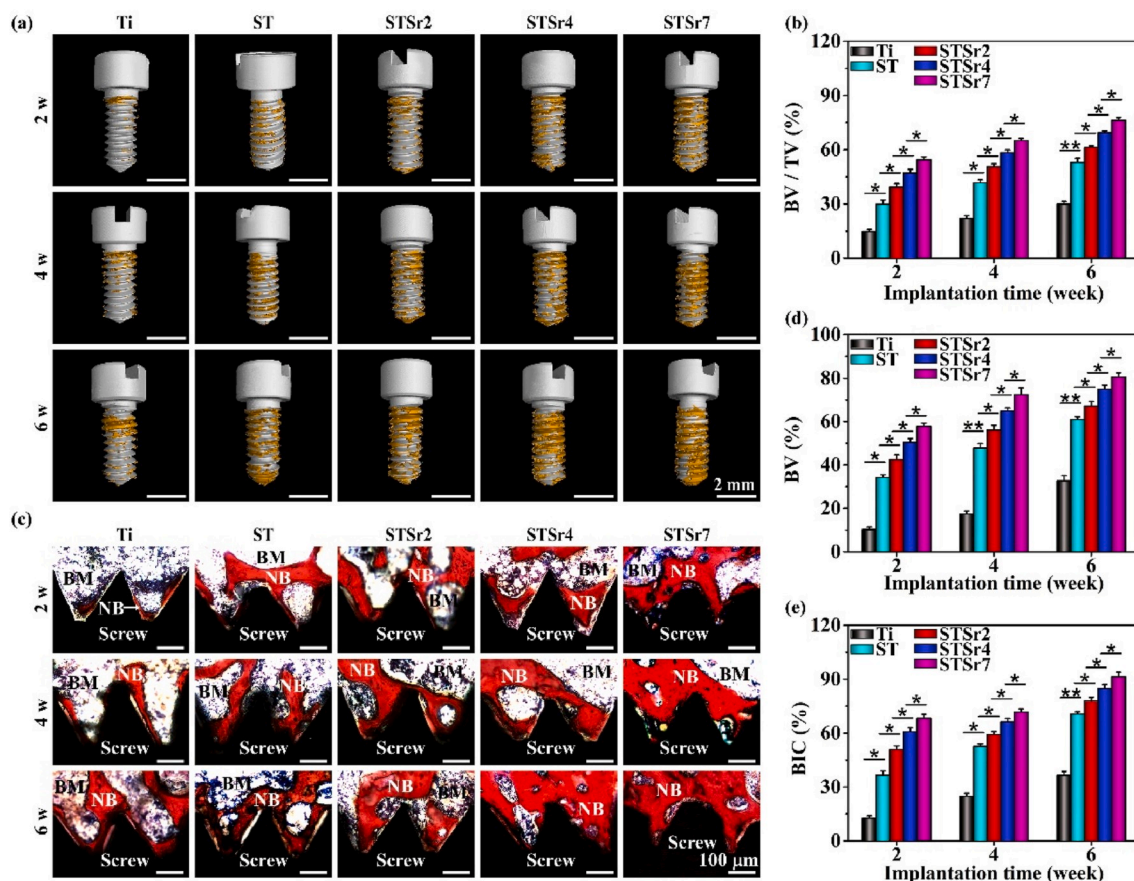


Fig. 8. Osseointegration of the nanorods-arrayed Ti and bare Ti screws after implantation in rat femoral condyles for different time: (a) Micro-CT images of the arrayed Ti and bare Ti (presented in white color) with surrounding new bone (presented in yellow color); (b) the quantitative ratios of new bone volume to total reconstructed peri-implant areas obtained from Micro-CT reconstruction; (c) histological stained images of peri-implant new bone; and (d) quantified percentage of new bone volumes (BV, %) as well as (e) corresponding contact ratios between new bone and screw (BIC, %) calculated from the stained images at implantation time of 2, 4 and 6 w (BM: bone marrow, NB: new bone). *p < 0.05, **p < 0.01.

higher mechanical resistance of peri-implant new bone, ensuring the early fixation between new bone and implants [21]. In addition, osteoid appears surrounding Sr-doped nanorods arrays, which increase with Sr incorporating amounts in the nanorods. After 4 weeks of implantation, a few of mature bone forms around Ti, while continuous and mature bone forms around these nanorods-patterned arrays, and its amounts follow the trend of STSr7, STSr4, STSr2 and ST. The newly formed bone increases around all the samples with prolonging implantation time to 6 weeks, and the new bone amounts surrounding each kind of the samples exhibit a similar trend to that at week 4, which is statistically presented in Fig. 7c and d. It is revealed that the Sr-doped arrays more pronouncedly enhance osteogenesis compared to ST and much more pronouncedly compared to Ti, and the enhancement is promoted with the increase of Sr incorporating amounts. The results are further confirmed by Micro-CT reconstruction after different implantation time, which are photographically and quantitatively shown in Fig. 8a and b. The new bone-implant contact ratios were assessed with VG staining, as shown in Fig. 8c–e. The Sr-doped nanorods arrays significantly enhance bone-implant contact in comparison with ST and much more significantly in comparison with Ti, following the sequence of STSr7, STSr4 and STSr2.

In summary, compared to ST, on one hand, the Sr-doped nanorods arrays accelerate phenotypic transformation of the adhered macrophages towards M2, leading to the upregulation of M2 macrophage secreted Arg-1, TGF- β 1 and BMP2 (Fig. 4), which facilitate recruitment and osteogenic differentiation of MC3T3 (Fig. 6). On the other hand, Sr²⁺ released from the Sr-doped nanorods arrays can directly promote osteogenic differentiation of the adhered osteogenesis-related cells (Fig. 5). Simultaneously, the enhancement of osteogenesis by the Sr-doped nanorods arrays according to paracrine of macrophages or direct effects on osteoblasts becomes more pronounced with the increase of Sr incorporating amounts in the arrays. Consequently, STSr7 exhibits the best performance in new bone apposition and thus osseointegration (Figs. 7 and 8).

4. Conclusions

To identify the modulation effects of Sr incorporating amounts in nanorods-patterned arrays on polarization behavior of macrophages and thus osseointegration, Na₂TiO₃ nanorods arrays with identical nanorod diameter of 65.10 ± 4.53 nm, length of 2.00 ± 0.15 μ m and inter-rod spacing value of 75.20 ± 4.64 nm but different Sr incorporating amounts were fabricated on Ti and termed as STSr2, STSr4 and STSr7, respectively, together with the array without Sr incorporation and bare Ti as controls. We identify that Sr is incorporated in Na₂TiO₃ lattice in the format of the substitution of Na⁺. The doped Sr exhibits a long-term release feature, and STSr7 releases higher Sr²⁺ amount compared to STSr4 and much higher compared to STSr2 within a same duration. The released Sr²⁺ enhances expressions of integrins subunits to promote the formation of focal adhesion, resulting in the enhanced adhesion and filopodia formation of macrophage on Sr doped arrays compared to those on Sr-free array. Consequently, compared to Sr-free array, Sr-doped arrays accelerate phenotypic transformation of macrophages towards M2, leading to the upregulated production of pro-osteogenic cytokines and growth factors (TGF- β 1 and BMP2). Moreover, the released Sr²⁺ can also directly enhance osteogenic functions of osteoblasts, MC3T3. Based on the enhanced role of Sr²⁺ in paracrine of M2 macrophages and osteogenic function of osteoblasts, Sr doped arrays show significantly enhanced osseointegration *in vivo* compared to the array without Sr incorporation, moreover, the enhancement is promoted with the increase of Sr incorporating amounts. Consequently, STSr7 exhibits the best performance in osseointegration *in vivo*. This work identifies the key role of Sr²⁺ incorporation into nanorods arrays on immunomodulation and its subsequent osseointegration, shedding a new light on the surface chemical and structural design for an orthopedic implant in favor of osteointegration.

Declaration of competing interest

All of the authors declare that there are no conflicts of interest.

CRediT authorship contribution statement

Dongmei Yu: Methodology, Investigation, Software, Formal analysis, Writing – original draft. **Shuo Guo:** Methodology, Investigation, Software, Visualization, Data curation. **Meng Yu:** Methodology, Investigation, Software, Visualization, Data curation. **Wenwen Liu:** Visualization, Validation, Software. **Xiaokang Li:** Methodology, Validation. **Dafu Chen:** Funding acquisition. **Bo Li:** Conceptualization, Writing – review & editing. **Zheng Guo:** Resources, Supervision. **Yong Han:** Conceptualization, Funding acquisition, Supervision, Writing – review & editing.

Acknowledgment

We appreciate Research Fund for the National Natural Science Foundation of China (Grant number 51631007, 51971171 and 31700860), and the joint project of Xi'an Jiaotong University and Beijing Research Institute of Traumatology and Orthopaedics (Contract No. 202012443) for financially supporting this work.

References

- [1] M.C.R. Alves-Rezende, L.C. Capalbo, J.P.J.D. Limirio, B.C. Capalbo, P.H.J. O. Limirio, J.L. Rosa, The role of TiO₂ nanotube surface on osseointegration of titanium implants: biomechanical and histological study in rats, *Microsc. Res. Tech.* 83 (2020) 817–823.
- [2] N. Jiang, Z.J. Guo, D. Sun, Y.B. Li, Y.T. Yang, C. Chen, L. Zhang, S.S. Zhu, Promoting osseointegration of Ti implants through micro/nanoscaled hierarchical Ti phosphate/Ti oxide hybrid coating, *ACS Nano* 12 (2018) 7883–7891.
- [3] Y.M. Niu, Z.Z. Wang, Y.C. Shi, L. Dong, C.M. Wang, Modulating macrophage activities to promote endogenous bone regeneration: biological mechanisms and engineering approaches, *Bioact. Mater.* 6 (2021) 244–261.
- [4] T.D. Smith, R.R. Nagalla, E.Y. Chen, W.F. Liu, Harnessing macrophage plasticity for tissue regeneration, *Adv. Drug Deliv. Rev.* 114 (2017) 193–205.
- [5] Y.J. Xie, C. Hu, Y. Feng, D.F. Li, T.T. Ai, Y.L. Huang, X.D. Chen, L.J. Huang, J. L. Tan, Osteoimmunomodulatory effects of biomaterial modification strategies on macrophage polarization and bone regeneration, *Regen. Biomater.* 7 (2020) 233–245.
- [6] J. Munoz, N.S. Akhavan, A.P. Mullins, B.H. Arjmandi, Macrophage polarization and osteoporosis: a review, *Nutrients* 12 (2020) 2999–3014.
- [7] A. Shapouri-Moghaddam, S. Mohammadian, H. Vazini, M. Taghadosi, S. A. Esmaili, F. Mardani, B. Seifi, A. Mohammadi, J.T. Afshari, A. Sahebkar, Macrophage plasticity, polarization, and function in health and disease, *J. Cell. Physiol.* 233 (2018) 6425–6440.
- [8] S.C. Funes, M. Rios, J. Escobar-Vera, A.M. Kalergis, Implications of macrophage polarization in autoimmunity, *Immunology* 154 (2018) 186–195.
- [9] H.W. Yang, M. Yu, R. Wang, B. Li, X. Zhao, Y.L. Hao, Z. Guo, Y. Han, Hydrothermally grown TiO₂-nanorods on surface mechanical attrition treated Ti: improved corrosion fatigue and osteogenesis, *Acta Biomater.* 116 (2020) 400–414.
- [10] S. Guo, D.M. Yu, X. Xiao, W.W. Liu, Z.G. Wu, L. Shi, Q.M. Zhao, D. Yang, Y.J. Lu, X. H. Wei, Z. Tang, N. Wang, X.K. Li, Y. Han, Z. Guo, A vessel subtype beneficial for osteogenesis enhanced by strontium-doped sodium titanate nanorods by modulating macrophage polarization, *J. Mater. Chem. B* 8 (2020) 6048–6058.
- [11] S.S. Jin, D.Q. He, D. Luo, Y. Wang, M. Yu, B. Guan, Y. Fu, Z.X. Li, T. Zhang, Y. H. Zhou, C.Y. Wang, Y. Liu, A biomimetic hierarchical nanointerface orchestrates macrophage polarization and mesenchymal stem cell recruitment to promote endogenous bone regeneration, *ACS Nano* 13 (2019) 6581–6595.
- [12] J. Lee, H. Byun, S.K.M. Perikamana, S. Lee, H. Shin, Current advances in immunomodulatory biomaterials for bone regeneration, *Adv. Healthc. Mater.* 8 (2019) 1801106–1801125.
- [13] S. Franz, S. Rammelt, D. Scharnweber, J.C. Simon, Immune responses to implants – a review of the implications for the design of immunomodulatory biomaterials, *Biomaterials* 32 (2011) 6692–6709.
- [14] G.Q. Chen, C.X. Deng, Y.P. Li, TGF- β and BMP signaling in osteoblast differentiation and bone formation, *Int. J. Biol. Sci.* 8 (2012) 272–288.
- [15] Z.T. Chen, C.T. Wu, W.Y. Gu, T. Klein, R. Crawford, Y. Xiao, Osteogenic differentiation of bone marrow MSCs by beta-tricalcium phosphate stimulating macrophages via BMP2 signalling pathway, *Biomaterials* 35 (2014) 1507–1518.
- [16] Q.L. Ma, L.Z. Zhao, R.R. Liu, B.Q. Jin, W. Song, Y. Wang, Y.S. Zhang, L.H. Chen, Y. M. Zhang, Improved implant osseointegration of a nanostructured titanium surface via mediation of macrophage polarization, *Biomaterials* 35 (2014) 9853–9867.
- [17] J.J. Wang, F.H. Meng, W. Song, J.Y. Jin, Q.L. Ma, D.D. Fei, L. Fang, L.H. Chen, Q. T. Wang, Y.M. Zhang, Nanostructured titanium regulates osseointegration via influencing macrophage polarization in the osteogenic environment, *Int. J. Nanomed.* 13 (2018) 4029–4043.

- [18] D.M. Yu, S. Guo, D. Yang, B. Li, Z. Guo, Y. Han, Interrod spacing dependent angiogenesis and osseointegration of Na₂TiO₃ nanorods-patterned arrays via immunoregulation, *Chem. Eng. J.* 426 (2021) 131187–131201.
- [19] Y.Z. Zhu, H. Liang, X.M. Liu, J. Wu, C. Yang, T.M. Wong, K.Y.H. Kwan, K.M. C. Cheung, S.L. Wu, K.W.K. Yeung, Regulation of macrophage polarization through surface topography design to facilitate implant-to-bone osteointegration, *Sci. Adv.* 7 (2021) eabf6654–eabf6667.
- [20] T.U. Luu, S.C. Gott, B.W.K. Woo, M.P. Rao, W.F. Liu, Micro- and nanopatterned topographical cues for regulating macrophage cell shape and phenotype, *ACS Appl. Mater. Interfaces* 7 (2015) 28665–28672.
- [21] B. Li, P. Gao, H.Q. Zhang, Z. Guo, Y.F. Zheng, Y. Han, Osteoimmunomodulation, osseointegration, and in vivo mechanical integrity of pure Mg coated with HA nanorod/pore-sealed MgO bilayer, *Biomater Sci-Uk* 6 (2018) 3202–3218.
- [22] C. Wang, B. Chen, W. Wang, X. Zhang, T. Hu, Y. He, K. Lin, X. Liu, Strontium released bi-lineage scaffolds with immunomodulatory properties induce a pro-regenerative environment for osteochondral regeneration, *Mater. Sci. Eng. C* 103 (2019) 109833–109844.
- [23] X.W. Yuan, H.L. Cao, J.X. Wang, K.W. Tang, B. Li, Y.C. Zhao, M.Q. Cheng, H. Qin, X.Y. Liu, X.L. Zhang, Immunomodulatory effects of calcium and strontium Co-doped titanium oxides on osteogenesis, *Front. Immunol.* 8 (2017) 1196–1210.
- [24] H. Yao, J. Xu, J. Wang, Y. Zhang, N. Zheng, J. Yue, J. Mi, L. Zheng, B. Dai, W. Huang, S. Yung, P. Hu, Y. Ruan, Q. Xue, K. Ho, L. Qin, Combination of magnesium ions and vitamin C alleviates synovitis and osteophyte formation in osteoarthritis of mice, *Bioact. Mater.* 6 (2021) 1341–1352.
- [25] B. Li, H.L. Cao, Y.C. Zhao, M.Q. Cheng, H. Qin, T. Cheng, Y. Hu, X.L. Zhang, X. Y. Liu, In vitro and in vivo responses of macrophages to magnesium-doped titanium, *Sci. Rep.* 7 (2017) 427077–442718.
- [26] W. Liu, J. Li, M. Cheng, Q. Wang, K.W.K. Yeung, P.K. Chu, X. Zhang, Zinc-modified sulfonated polyetheretherketone surface with immunomodulatory function for guiding cell fate and bone regeneration, *Adv. Sci.* 5 (2018) 1800749–1800761.
- [27] J. Gong, M. Sun, S. Wang, J. He, Y. Wang, Y. Qian, Y. Liu, L. Dong, L. Ma, K. Cheng, W. Weng, M. Yu, Y.S. Zhang, H. Wang, Surface modification by divalent main-group-elemental ions for improved bone remodeling to instruct implant biofabrication, *ACS Biomater. Sci. Eng.* 5 (2019) 3311–3324.
- [28] F.J. Zhao, B. Lei, X. Li, Y.F. Mo, R.X. Wang, D.F. Chen, X.F. Chen, Promoting in vivo early angiogenesis with sub-micrometer strontium-contained bioactive microspheres through modulating macrophage phenotypes, *Biomaterials* 178 (2018) 36–47.
- [29] W. Zhang, F. Zhao, D. Huang, X. Fu, X. Li, X. Chen, Strontium-Substituted submicrometer bioactive glasses modulate macrophage responses for improved bone regeneration, *ACS Appl. Mater. Interfaces* 8 (2016) 30747–30758.
- [30] D.W. Zhao, C. Liu, K.Q. Zuo, P. Su, L.B. Li, G.Y. Xiao, L. Cheng, Strontium-zinc phosphate chemical conversion coating improves the osseointegration of titanium implants by regulating macrophage polarization, *Chem. Eng. J.* 408 (2021) 127362–127380.
- [31] S. Yamaguchi, S. Nath, T. Matsushita, T. Kokubo, Controlled release of strontium ions from a bioactive Ti metal with a Ca-enriched surface layer, *Acta Biomater.* 10 (2014) 2282–2289.
- [32] G.S. Wang, Y. Wan, B. Ren, T. Wang, Z.Q. Liu, Surface functionalization of micro/nanostructured titanium with bioactive ions to regulate the behaviors of murine osteoblasts, *Adv. Eng. Mater.* 19 (2017) 1700299–1700309.
- [33] J. Braux, F. Velard, C. Guillaume, S. Bouthors, E. Jallot, J.M. Nedelec, D. Laurent-Maquin, P. Laquerriere, A new insight into the dissociating effect of strontium on bone resorption and formation, *Acta Biomater.* 7 (2011) 2593–2603.
- [34] Z. Saidak, P.J. Marie, Strontium signaling: molecular mechanisms and therapeutic implications in osteoporosis, *Pharmacol. Therapeut.* 136 (2012) 216–226.
- [35] J. Yan, J.F. Sun, P.K. Chu, Y. Han, Y.M. Zhang, Bone integration capability of a series of strontium-containing hydroxyapatite coatings formed by micro-arc oxidation, *J. Biomed. Mater. Res.* 101 (2013) 2465–2480.
- [36] E. Buache, F. Velard, E. Bauden, C. Guillaume, E. Jallot, J.M. Nedelec, D. Laurent-Maquin, P. Laquerriere, Effect of strontium-substituted biphasic calcium phosphate on inflammatory mediators production by human monocytes, *Acta Biomater.* 8 (2012) 3113–3119.
- [37] P. Romer, B. Desaga, P. Proff, A. Faltermeier, C. Reicheneder, Strontium promotes cell proliferation and suppresses IL-6 expression in human PDL cells, *Ann. Anat.* 194 (2012) 208–211.
- [38] H.B. Pan, Z.Y. Li, W.M. Lam, J.C. Wong, B.W. Darvell, K.D.K. Luk, W.W. Lu, Solubility of strontium-substituted apatite by solid titration, *Acta Biomater.* 5 (2009) 1678–1685.
- [39] Y. Ishikawa, S. Tsukimoto, K.S. Nakayama, N. Asao, Ultrafine sodium titanate nanowires with extraordinary Sr ion-exchange properties, *Nano Lett.* 15 (2015) 2980–2984.
- [40] Z. Esen, E.B. Ocal, Surface characteristics and in-vitro behavior of chemically treated bulk Ti6Al7Nb alloys, *Surf. Coating. Technol.* 309 (2017) 829–839.
- [41] T. Svitkina, The actin cytoskeleton and actin-based motility, *Cold Spring Harb. Perspect. Biol.* 10 (2018) a018267–a018288.
- [42] J.H. Zhou, Y. Han, S.M. Lu, Direct role of interrod spacing in mediating cell adhesion on Sr-HA nanorod-patterned coatings, *Int. J. Nanomed.* 9 (2014) 1243–1260.
- [43] S.M. Choi, J.W. Park, Multifunctional effects of a modification of SLA titanium implant surface with strontium-containing nanostructures on immunoinflammatory and osteogenic cell function, *J. Biomed. Mater. Res.* 106 (2018) 3009–3020.
- [44] J.W. Park, Y.J. Kim, J.H. Jang, J.Y. Suh, Surface characteristics and primary bone marrow stromal cell response of a nanostructured strontium-containing oxide layer produced on a microrough titanium surface, *J. Biomed. Mater. Res.* 100A (2012) 1477–1487.
- [45] M. Li, P. He, Y.H. Wu, Y. Zhang, H. Xia, Y.F. Zheng, Y. Han, Stimulatory effects of the degradation products from Mg-Ca-Sr alloy on the osteogenesis through regulating ERK signaling pathway, *Sci. Rep.* 6 (2016) 32323–32335.
- [46] J.H. Zhou, L.Z. Zhao, Hypoxia-mimicking Co doped TiO₂ microporous coating on titanium with enhanced angiogenic and osteogenic activities, *Acta Biomater.* 43 (2016) 358–368.
- [47] Z.T. Chen, T. Klein, R.Z. Murray, R. Crawford, J. Chang, C.T. Wu, Y. Xiao, Osteoimmunomodulation for the development of advanced bone biomaterials, *Mater. Today* 19 (2016) 304–321.
- [48] C. Gamell, N. Osses, R. Bartrons, T. Rueckle, M. Camps, J.L. Rosa, F. Ventura, BMP2 induction of actin cytoskeleton reorganization and cell migration requires PI3-kinase and Cdc 42 activity, *J. Cell Sci.* 121 (2008) 3960–3970.
- [49] P. Zhou, D. Xia, Z. Ni, T. Ou, Y. Wang, H. Zhang, L. Mao, K. Lin, S. Xu, J. Liu, Calcium silicate bioactive ceramics induce osteogenesis through oncostatin M, *Bioact. Mater.* 6 (2021) 810–822.
- [50] E. Chen, G. Liu, X. Zhou, W. Zhang, C. Wang, D. Hu, D. Xue, Z. Pan, Concentration-dependent, dual roles of IL-10 in the osteogenesis of human BMSCs via P38/MAPK and NF-kappaB signaling pathways, *Faseb. J.* 32 (2018) 4917–4929.